

Elastic turbulence in highly entangled polymers and wormlike micelles

Theo A. Lewy,^{1,*} Suzanne M. Fielding,² Peter D. Olmsted,³ and Rich R. Kerswell¹

¹*DAMTP, University of Cambridge, Cambridge CB3 0WA, UK*

²*Department of Physics, Durham University, Science Laboratories, South Road, Durham DH1 3LE, UK*

³*Department of Physics and Institute for Soft Matter Synthesis & Metrology, Georgetown University, Washington DC 20057, USA*

We show theoretically that an initially homogeneous planar Couette flow of a concentrated polymeric fluid is linearly unstable to the growth of two-dimensional (2D) perturbations, within two widely used constitutive models: the Johnson-Segalman model and the Rolie-Poly model. We perform direct nonlinear simulations of both models in 2D to show that this instability leads to a state of elastic turbulence comprising several narrow shear bands that dynamically coalesce, split and interact. Importantly, we show that this 2D instability arises not only in fluids that have a non-monotonic constitutive curve, and therefore show shear banding in 1D calculations, but also in shear thinning fluids with a monotonic constitutive curve, for which an initially homogeneous base state is stable in 1D. For the former category, the high shear branch of the constitutive curve is unstable to 2D instability in both models, so that the high shear band may be turbulent. In the Rolie-Poly model, the low shear branch is also likewise unstable. Our work provides the first simulation evidence for elastic turbulence in highly entangled polymeric fluids. It also potentially explains rheo-chaotic states seen experimentally in shear banding wormlike micelles. We additionally demonstrate elastic turbulence within both models in the planar Poiseuille geometry.

Polymeric fluids show strongly nonlinear flow phenomena that significantly impact industrial processes such as the extrusion and moulding of molten plastics [1]. At a microscopic level, chainlike polymer molecules show sluggish viscoelastic relaxation dynamics and are easily disturbed by an imposed flow. Beyond a critical value of the Weissenberg number, defined as the ratio of flow rate to viscoelastic relaxation rate, this leads to nonlinear and unstable flow phenomena at the macroscopic level, even at negligible Reynolds number.

Dilute polymer solutions have long been known to suffer linear instabilities driven by hoop stresses in flow geometries with curved streamlines [2–4], with a pathway to elastic turbulence (ET) at high Weissenberg number [5, 6]. ET has also been observed in dilute solutions in rectilinear geometries: experimentally in channels [7–9] and pipes [10], and numerically in Kolmogorov flow [11–13], channels [14, 15] and plane Couette flow [16, 17]. The instabilities that underlie ET in dilute solutions are predicted to arise either linearly via a hoop stress [2], centre-mode [18–21] or polymer diffusive [16, 22, 23] mechanism, or via finite-amplitude perturbations [24, 25].

Whereas in dilute solutions the chainlike molecules behave independently, in concentrated solutions and melts they can be highly entangled with each other. Surprisingly, ET in these systems remains significantly underexplored to date. The central contribution of this Letter is to demonstrate ET for the first time in direct numerical simulations of concentrated shear thinning polymeric fluids. We study two widely used constitutive models in two rectilinear geometries, which lack hoop stresses in any initially laminar base state: planar Poiseuille flow (pPf), in which the base state has significant stress gradients, and planar Couette flow (pCf), in which the base state has uniform stress. We also identify a route to ET

via the linear instability of an initially rectilinear base state. In pPf, this is consistent with existing predictions that normal stress gradients can cause instability in shear thinning fluids [26–29], as seen experimentally [30–32]. Early work also predicted linear instability of the shear thinning Phan-Thien-Tanner model in pCf [29], but without making any link with ET. Indeed, our finding of ET in concentrated polymeric fluids in a flow geometry that lacks either hoop stresses or stress gradients is particularly unexpected.

In concentrated polymers [33, 34] and wormlike micellar surfactants [35], an initially homogeneous shear flow is often unstable to the formation of coexisting bands of differing shear rate, with layer normals in the flow-gradient direction. This instability is driven by a region of negative slope in the underlying constitutive relation between shear stress and shear rate, such that the constitutive curve as a whole is non-monotonic [36]. In addition to our work demonstrating ET in fluids with a monotonic constitutive curve, a significant additional contribution of this Letter is to uncover ET in shear banding fluids with a non-monotonic constitutive curve, again by means of both linear stability analysis and nonlinear simulations.

Indeed, experiments on shear banded flows commonly reveal ET [37–39], with the high shear band often turbid [40–45] and chaotic [46, 47]. Historically, however, shear banded states have often been interpreted via one-dimensional (1D) calculations predicting a flat interface between stationary homogeneous bands [48–50]. Early attempts to capture complex spatiotemporal dynamics suggested possible ‘rheo-chaos’ of the high shear band [51], concentration coupling [52], or an undulatory instability of the banding interface [53–55]. Importantly, our work suggests that many experiments should instead be interpreted in terms of the coexistence of an elasti-

cally turbulent high shear band with a laminar low shear band.

Models — We consider incompressible flow that satisfies $\nabla \cdot \mathbf{u} = 0$, and the inertialess force balance equation:

$$0 = \mu \nabla^2 \mathbf{u} + \nabla \cdot \boldsymbol{\Sigma} - \nabla p - G \hat{\mathbf{x}}, \quad (1)$$

with velocity \mathbf{u} , solvent viscosity μ , polymer stress $\boldsymbol{\Sigma}$ and pressure p . The imposed pressure gradient $G \neq 0$ in pPf and $G = 0$ in pCf. For the polymer stress, we consider two widely used constitutive models of entangled polymeric fluids: the phenomenological Johnson-Segalman (JS) model [56] and the microscopically motivated Rolie-Poly (RP) model [57]. Both capture shear thinning and, in some parameter regimes, shear banding and can be written in the same compact way:

$$\overset{\circ}{\boldsymbol{\Sigma}} = 2G_p \mathbf{D} - \frac{2}{\tau_R} (1 - A)(\mathbf{I} + \boldsymbol{\Sigma} + \beta A \boldsymbol{\Sigma}) - \frac{\boldsymbol{\Sigma}}{\tau_d} + \mathcal{D} \nabla^2 \boldsymbol{\Sigma}, \quad (2)$$

with the Gordon-Schowalter time derivative [58]

$$\overset{\circ}{\boldsymbol{\Sigma}} := \frac{\partial \boldsymbol{\Sigma}}{\partial t} + \mathbf{u} \cdot \nabla \boldsymbol{\Sigma} - a(\boldsymbol{\Sigma} \cdot \mathbf{D} + \mathbf{D} \cdot \boldsymbol{\Sigma}) - (\boldsymbol{\Sigma} \cdot \boldsymbol{\Omega} - \boldsymbol{\Omega} \cdot \boldsymbol{\Sigma}).$$

Here \mathbf{D} and $\boldsymbol{\Omega}$ denote the symmetric and antisymmetric parts of the velocity gradient tensor $(\nabla \mathbf{u})_{ij} = \partial_i u_j$. Both models have a polymer modulus G_p , reptation time τ_d and stress diffusion coefficient \mathcal{D} . The JS model obtains for $\tau_R \rightarrow \infty$, with β then irrelevant, and has a slip parameter a with $|a| < 1$. The RP model has a constraint release parameter β and Rouse time τ_R , with $A := (1 + \text{tr}(\boldsymbol{\Sigma})/3)^{-1/2}$, and obtains for $a = 1$.

Flow geometry — We consider two-dimensional (2D) flow in the x - y plane, with flow direction $\hat{\mathbf{x}}$ and flow-gradient direction $\hat{\mathbf{y}}$. We assume translational invariance in the vorticity direction $\hat{\mathbf{z}}$ ($\partial_z = 0$), with $u_z = 0$ and $\Sigma_{xz} = \Sigma_{yz} = 0$. Our flow domain is bounded by hard flat plates at $y = \pm h$, where we assume boundary conditions of no-penetration and no-slip for the velocity. In pCf this gives $\mathbf{u}|_{\pm h} = \pm U_0 \hat{\mathbf{x}}$ where U_0 is the magnitude of the plate speed. In pPf it gives $\mathbf{u}|_{\pm h} = \mathbf{0}$. Non-zero stress diffusion \mathcal{D} also requires a boundary condition on $\boldsymbol{\Sigma}$. Unless otherwise stated we use the Neumann condition $\partial_y \boldsymbol{\Sigma}|_{\pm h} = \mathbf{0}$. However, we have checked robustness by also considering $\nabla^2 \boldsymbol{\Sigma}|_{\pm h} = \mathbf{0}$, equivalent to enforcing $\mathcal{D} = 0$ at the walls [59].

Units and parameter values — We choose units in which the polymer modulus $G_p = 1$, reptation time $\tau_d = 1$ and channel half-height $h = 1$. We set the dimensionless stress diffusion coefficient $\varepsilon := \mathcal{D} \tau_d / h^2 = 10^{-3}$ throughout. In the RP model we also set the constraint release parameter $\beta = 0.71$ [60]. We then vary the slip parameter a in the JS model, the entanglement number $Z := \tau_d / 3 \tau_R$ in the RP model, and the dimensionless solvent viscosity ratio $\delta := \mu / \tau_d G_p$ in both models in a regime of high polymer concentration, $\delta \ll 1$. We also

vary the Weissenberg number $W := U_0 \tau_d / h$ (in pCf) or pressure gradient G (in pPf).

Linear stability analysis — We first examine the stability of an initial base state of homogeneous pCf, with uniform polymer stress $\boldsymbol{\Sigma}$ and shear rate $\dot{\gamma}$, with respect to small amplitude heterogeneous perturbations $\delta \boldsymbol{\Sigma}, \delta \dot{\gamma}$ that depend on x and t as $e^{ik(x-ct)}$, as well as on y . Here $k \in \mathbb{R}$ is the streamwise wavenumber and $c \in \mathbb{C}$ is a complex wave speed to be found. We define the growth rate $\omega := kc_i$, where $c_i := \text{Im} c$, so that modes with $\omega > 0$ are linearly unstable. The largest growth rate for purely 1D perturbations (which depend only on y) is defined as $\omega_{1D} := \omega(k = 0)$ while the most unstable growth rate over all k is defined as $\omega^* := \sup_{k \in \mathbb{R}} \omega(k)$. Hence $\omega^* \geq \omega_{1D}$, with $\omega^* = \omega_{1D}$ when 1D perturbations are the most unstable.

Constitutive curves of shear stress as a function of shear rate are shown in Figs. 1a and 1b for the JS and RP models respectively. An initial state of homogeneous pCf (the ‘0D’ state) is known to be unstable to the growth of 1D perturbations in the regime of negative constitutive slope, leading to the formation of shear bands with layer normals along y [36]. We indeed find $\omega_{1D} > 0$ in this regime, in both JS and RP. Interestingly, however, we find purely 1D perturbations to be more unstable than 2D ones only in the JS model at relatively low shear rates: $0 < \omega^* = \omega_{1D}$, as shown by the red lines in Fig. 1a. Throughout the rest of the regime of negative slope in JS, and all of this regime in RP, 2D perturbations are more unstable: $0 < \omega_{1D} < \omega^*$, as shown by the green lines in Fig. 1a,b.

More interestingly still, in both JS and RP we find that 2D perturbations can grow even in regimes of positive constitutive slope, where 1D perturbations are stable: $\omega_{1D} < 0 < \omega^*$ (blue lines in Fig. 1a,b). In the JS model, this 2D instability arises only on the high shear branch of the constitutive curve, above the regime of negative constitutive slope. In the RP model, it arises on both the high and low shear branches, either side of the window of negative slope. Importantly, the RP model shows this 2D instability even at low entanglement numbers, for which the constitutive curve is monotone increasing, giving shear thinning but not shear banding.

At larger W in the JS model, the 2D instability changes in character, from having an eigenfunction that is global and large scale, corresponding to a bulk constitutive instability, to being small scale and confined to the boundary, corresponding to a polymer diffusive instability (PDI) [16, 22, 23]). (This switch is identified via a discontinuity in the most unstable wavenumber k^* . See Fig. 4a of Appendix A.) No PDI arises in the RP model: its 2D instability is always a bulk constitutive mode.

The instability regimes just discussed in the context of the constitutive curves are summarised in the parameter planes of a - W (for JS) and Z - W (RP) in Figs. 1c,d with the same colour coding as in Figs. 1a,b. In both models,

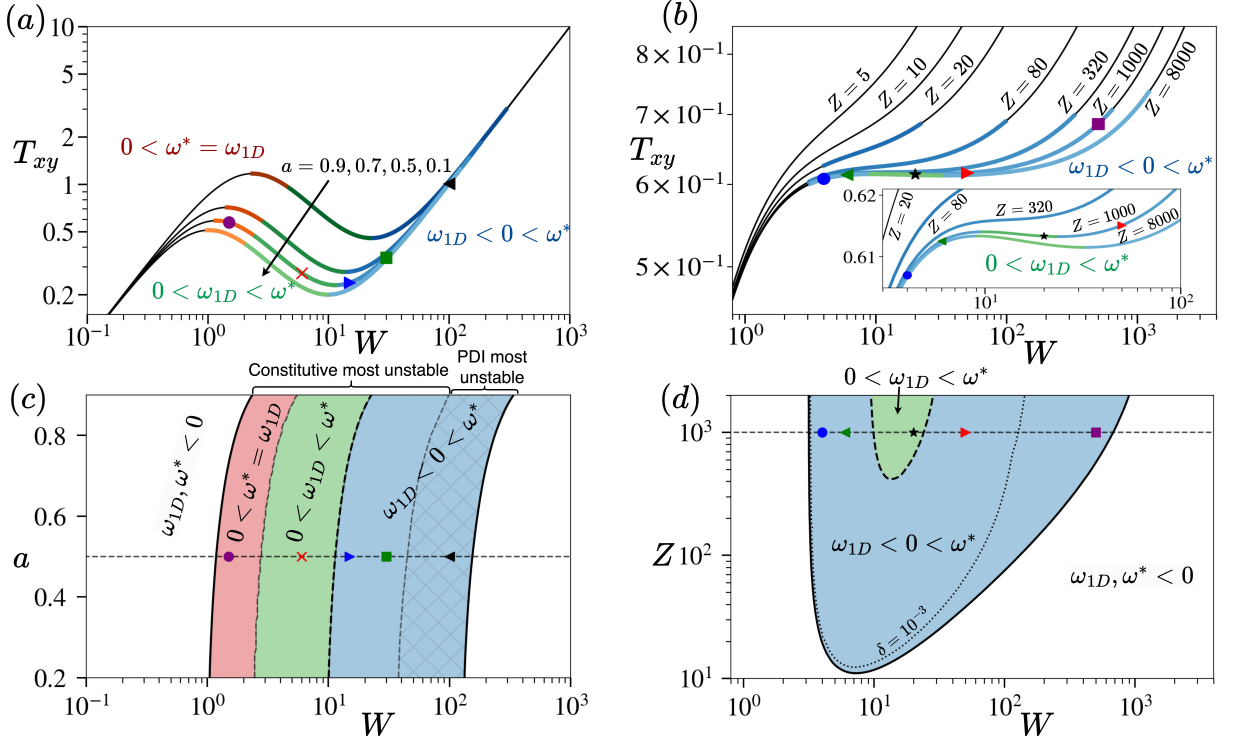


FIG. 1. Constitutive curves and stability maps in pCf of the JS model with $\delta = 10^{-2}$, $\varepsilon = 10^{-3}$ and of the RP model with $\delta = 10^{-4}$, $\varepsilon = 10^{-3}$. (a) Constitutive curves of the JS model for several values of a . (b) Constitutive curves of the RP model for several values of Z . (c) Stability map of the JS model in the a - W plane. (d) Stability map of the RP model in the Z - W plane. Colours show linear instabilities with $0 < \omega^* = \omega_{1D}$ (red), $0 < \omega_{1D} < \omega^*$ (green) and $\omega_{1D} < 0 < \omega^*$ (blue). Hatching for the JS model in c) shows regions where the PDI is the most unstable mode. The PDI does not arise for the RP model in d). The dotted line in d) additionally shows the neutral curve when $\delta = 10^{-3}$. Dispersion relations and most unstable eigenmodes at symbols along the horizontal dashed lines in (c) at $a = 0.5$ and in (d) at $Z = 1000$ are shown in Fig. 4 in the End Matter.

the large blue regions of parameter space are particularly striking, as they indicate regimes of 2D *instability* in which the constitutive curve nonetheless has positive slope, giving 1D *stability*. We subdivide these blue regions into unhatched, to denote the bulk constitutive instability, and hatched, to denote the PDI (present only in JS).

Shear thinning polymeric fluids were previously shown to be linearly unstable to the growth of 2D perturbations within several constitutive models [26–29]. However, those works focused mostly on pressure driven flow, pPf, and suggest the instability to be driven by gradients in the base state’s normal stress. In significant contrast, we report 2D instability here in the JS and RP models in pCf, for which the base state is homogeneous, consistent with an early report of 2D instability of pCf in the Phan-Thien-Tanner model of concentrated polymers [29].

Elastic Turbulence — So far, we have shown by means of linear stability analysis that a state of initially homogeneous pCf suffers a 2D constitutive instability in the large regimes of parameter space shown by the blue unhatched regions in Figs. 1c,d. We now perform direct nonlinear simulations to evolve this 2D instability to fi-

nite amplitude in a domain of length $L_x = 2\pi$, using the spectral codebase Dedalus [61]. In both the JS and RP models, this will reveal chaotic dynamics that we identify as ET. (For justification of our classification of any state as chaotic or quasi-periodic, see Fig. 3). For comparison, we shall also perform 1D nonlinear simulations with spatial variations only in y .

In both 1D and 2D, we simulate a ramp-down protocol that starts at a high Weissenberg number $W = 20.0$, and progressively steps W downwards, waiting at each W for times $t_w = 200$ ($t_w = 500$ for $W < 5.0$) to ensure that the space-averaged total shear stress $T_{xy} = \Sigma_{xy} + \eta\dot{\gamma}$ attains a statistically steady state, as evidenced in Fig. 3. Convergence checks at $W = 20.0$ in both models confirmed that numbers of Fourier-Chebyshev modes $(N_x, N_y) = (400, 400)$ and $(600, 600)$ give results with less than 0.5% difference in the time- and space-averaged \bar{T}_{xy} . For the JS (resp. RP) model we used the latter (resp. former) spatial resolution with timestep $dt = 10^{-4}$ (resp. 5×10^{-5}), checking for convergence by halving the timestep.

The flow curve $\bar{T}_{xy}(W)$ obtained in 2D simulations of the JS model is shown by the blue line in Fig. 2a, with the

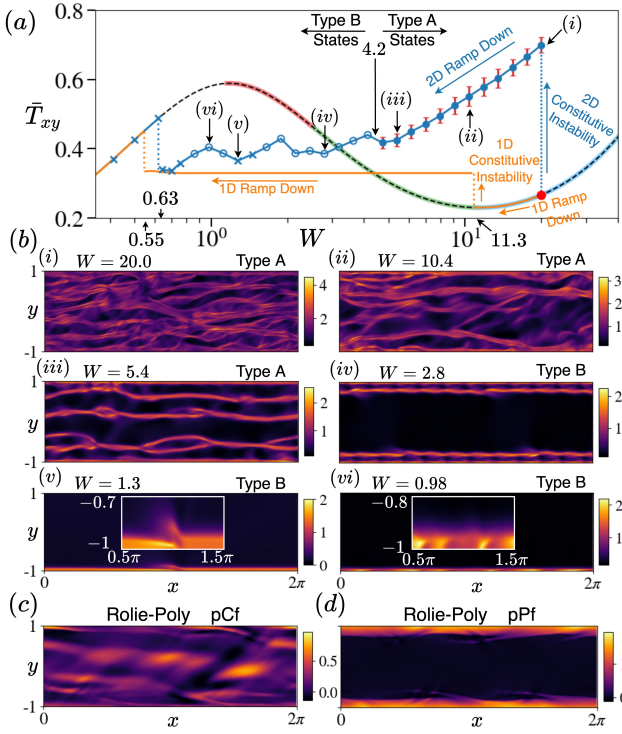


FIG. 2. (a) Flow curves obtained by ramping down the shear rate within the JS model in pCf: in 2D (solid blue line), 1D (solid orange line) and 0D (black dashed lines). In each case the initial condition comprises a state of homogeneous shear at $W = 20$ (red circle). In the 2D simulations, steady stress values are shown by crosses and fluctuating stress values by closed (resp. open) circles for standard deviations larger (resp. smaller) than 0.01, with vertical red bars showing ± 1 standard deviation. Linear stability regimes of the 0D curve are marked by colours as in Fig. 1a. $a = 0.5$, $\delta = 10^{-2}$, $\varepsilon = 10^{-3}$. (b) Snapshots of the trace $\Sigma_{xx} + \Sigma_{yy} + \Sigma_{zz}$ of the polymer stress for states marked (i)–(vi) in (a). (c) Snapshot of the trace of the polymer stress in the RP model in pCf for $W = 20$ and $Z = 50$, $\delta = 10^{-3}$, $\varepsilon = 10^{-3}$. (d) Counterpart for the RP model in pPf for $G = -1$. Timeseries and frequency spectra of the stress signals are shown in Fig. 3.

underlying homogeneous constitutive curve shown by the black dashed line for comparison. Representative snapshots of the states, characterised by the trace of the polymer stress, are shown in (b) for the values of W indicated (i)–(vi) in (a). We identify ET with two qualitatively different types of state: type A for $W > 4.2$ and type B for $W < 4.2$.

Type A states comprise multiple bands arranged across the flow gradient direction, each with a 2D structure. See snapshots (i)–(iii) in Fig. 2b. The number of bands fluctuates over time as they dynamically coalesce and split. The associated stress signal is chaotic, with standard deviation shown by the vertical red bars in Fig. 2a.

Type B states comprise distinct bands that are localised near the domain walls. Their number remains constant over time, with each band a coherently distinct

entity. The shear stress fluctuates less than for type A states, being either constant (crosses in Fig. 2a) or with standard deviation less than 0.01 (open circles). For $W = 2.8$ (snapshot *iv*) we find four bands with quasi-periodic dynamics. At lower W we find a single thin band, still with some 2D structure, exhibiting a traveling wave at $W = 1.3$ (snapshot *v*) or chaos at $W = 0.98$ (snapshot *vi*). Homogeneous flow is recovered for $W < 0.63$.

The flow curve obtained in 1D ramp-down simulations is shown by the orange line for comparison. It follows the well-known scenario of 1D shear banding calculations [50]. For $W > 11.3$ and $W < 0.55$ the flow curve coincides with the constitutive curve and the shear field is homogeneous. For $0.55 < W < 11.3$ the flow curve shows a flat plateau of constant stress T_{xy} and the flow field is shear banded. (For shear rates just to the left (resp. right) of the negative slope in the constitutive curve, where the stress is greater (resp. less) than the plateau value, states of homogeneous shear are known to be metastable [62].)

A 1D state with a flat interface between shear bands is known to suffer an interfacial instability [53, 55]. In a state with just two bands, this leads to undulations along the banding interface [63]. When multiple bands are present (Fig. 5 of Ref. [63]), it leads to a state suggestive of low dimensional chaos. These states reported in Ref. [63] resemble our type B states in Fig. 2b (iv–vi). Plausibly, the 2D constitutive instability of an initial state of homogeneous pCf reported here takes a system directly to the states obtained via the 2D interfacial instability of an initially 1D shear banded state in Ref. [53]. No counterpart of our type A states showing broadband turbulence was obtained in Ref. [63].

So far, we have demonstrated ET in the flow geometry of pCf, within the JS model, and with a non-monotonic constitutive curve. We show finally that ET arises robustly across different flow geometries (pCf vs. pPf), constitutive models (JS vs. RP) and shapes of constitutive curve (non-monotonic vs. monotonic). For example, Fig. 2c shows ET in the RP model at parameter values for which the constitutive curve is monotonic. Importantly, this shows that ET can arise in concentrated polymeric fluids that are shear thinning but not susceptible to (1D) shear banding. We also found ET in pPf, for which the base state stress T_{xy} is heterogeneous, with the turbulent region close to the channel walls: for $G = -1$, $a = 0.5$, $\delta = 10^{-2}$, $\varepsilon = 10^{-3}$ in the JS model (not shown) and in Fig. 2d for the RP model.

Discussion.— In this Letter, we have identified that two widely used constitutive models of concentrated polymeric fluids are susceptible to the 2D instability found for shear thinning fluids in [29]. We have further shown that this triggers 2D ET. This is the first numerical demonstration of ET in concentrated polymeric fluids, and it is robust to change in model (JS and RP) and geometry (pCf and pPf). Importantly, ET arises for

both monotonic shear thinning and non-monotonic shear banding constitutive curves. In the latter, 2D instability occurs on the high shear branch of both JS and RP models considered, as well as the low shear branch in the RP model.

Further work is required to see how closely the ET identified here matches experiment. In the Taylor-Couette geometry, constitutive and hoop stress instabilities [64] coexist, and it is commonly thought that the latter is responsible for instabilities on the high shear branch [37–39]. However, when the curvature is low and hoop stresses are weak (or absent in rectilinear systems), the constitutive instability is more important and may give rise to a different ET state compared to the hoop stress instability. Calculations in a Taylor-Couette geometry would be a useful next step in identifying the relevance of the constitutive ET, with an investigation of 3D effects allowing for more concrete comparison with experiments. Our findings suggest that the shear banded states observed in wormlike micelles and polymer solutions may comprise a homogeneous low shear rate band co-existing with a turbulent high shear band, in contrast to the simpler 1D interpretation of banding between homogenous stable states [49]. This may explain the so-called ‘rheo-chaos’ observed experimentally by Sood *et al.* [46, 47].

Acknowledgements.— PDO is grateful to Georgetown University and the Ives Foundation for financial support. This project has received funding from the European Research Council (ERC) under the European Union’s Horizon 2020 research and innovation programme (grant agreement No. 885146).

* tal43@cam.ac.uk

- [1] R. G. Larson, Instabilities in viscoelastic flows, *Rheologica Acta* **31**, 213 (1992).
- [2] R. G. Larson, E. S. Shaqfeh, and S. J. Muller, A purely elastic instability in taylor–couette flow, *Journal of Fluid Mechanics* **218**, 573 (1990).
- [3] D. O. Olagunju, Elastic instabilities in cone-and-plate flow: small gap theory, *Zeitschrift für angewandte Mathematik und Physik ZAMP* **46**, 946 (1995).
- [4] P. Pakdel and G. H. McKinley, Elastic instability and curved streamlines, *Physical Review Letters* **77**, 2459 (1996).
- [5] B. A. Schiamborg, L. T. Shereda, H. Hu, and R. G. Larson, Transitional pathway to elastic turbulence in torsional, parallel-plate flow of a polymer solution, *Journal of Fluid Mechanics* **554**, 191 (2006).
- [6] A. Groisman and V. Steinberg, Elastic turbulence in a polymer solution flow, *Nature* **405**, 53 (2000).
- [7] L. Pan, A. Morozov, C. Wagner, and P. E. Arratia, Non-linear elastic instability in channel flows at low Reynolds numbers, *Phys. Rev. Lett.* **110**, 174502 (2013).
- [8] B. Qin and P. E. Arratia, Characterizing elastic turbulence in channel flows at low Reynolds number, *Phys. Rev. Fluids* **2**, 083302 (2017).
- [9] R. Shnapp and V. Steinberg, Nonmodal elastic instability and elastic waves in weakly perturbed channel flow, *Phys. Rev. Fluids* **7**, 063901 (2022).
- [10] D. Bonn, F. Ingremau, Y. Amarouchene, and H. Kellay, Large velocity fluctuations in small-Reynolds-number pipe flow of polymer solutions, *Phys. Rev. E* **84**, 045301 (2011).
- [11] S. Berti, A. Bistagnino, G. Boffetta, A. Celani, and S. Musacchio, Two-dimensional elastic turbulence, *Phys. Rev. E* **77**, 055306 (2008).
- [12] S. Berti and G. Boffetta, Elastic waves and transition to elastic turbulence in a two-dimensional viscoelastic Kolmogorov flow, *Phys. Rev. E* **82**, 036314 (2010).
- [13] T. Lewy and R. R. Kerswell, Revisiting two-dimensional viscoelastic Kolmogorov flow: a centre-mode-driven transition, *Journal of Fluid Mechanics* **1007**, A55 (2025).
- [14] G. Foggi Rota, C. Amor, S. Le Clainche, and M. E. Rosti, Unified view of elastic and elasto-inertial turbulence in channel flows at low and moderate Reynolds numbers, *Phys. Rev. Fluids* **9**, L122602 (2024).
- [15] M. Lellep, M. Linkmann, and A. Morozov, Purely elastic turbulence in pressure-driven channel flows, *Proceedings of the National Academy of Sciences* **121**, e2318851121 (2024).
- [16] M. Beneitez, J. Page, and R. R. Kerswell, Polymer diffusive instability leading to elastic turbulence in plane Couette flow, *Phys. Rev. Fluids* **8**, L101901 (2023).
- [17] M. Beneitez, J. Page, Y. Dubief, and R. R. Kerswell, Transition route to elastic and elasto-inertial turbulence in polymer channel flows, *Phys. Rev. Fluids* **9**, 123302 (2024).
- [18] P. Garg, I. Chaudhary, M. Khalid, V. Shankar, and G. Subramanian, Viscoelastic pipe flow is linearly unstable, *Phys. Rev. Lett.* **121**, 024502 (2018).
- [19] I. Chaudhary, P. Garg, G. Subramanian, and V. Shankar, Linear instability of viscoelastic pipe flow, *Journal of Fluid Mechanics* **908**, A11 (2021).
- [20] M. Khalid, I. Chaudhary, P. Garg, V. Shankar, and G. Subramanian, The centre-mode instability of viscoelastic plane Poiseuille flow, *Journal of Fluid Mechanics* **915**, A43 (2021).
- [21] M. Khalid, V. Shankar, and G. Subramanian, Continuous pathway between the elasto-inertial and elastic turbulent states in viscoelastic channel flow, *Phys. Rev. Lett.* **127**, 134502 (2021).
- [22] T. Lewy and R. R. Kerswell, The polymer diffusive instability in highly concentrated polymeric fluids, *Journal of Non-Newtonian Fluid Mechanics* **326**, 105212 (2024).
- [23] M. M. Couchman, M. Beneitez, J. Page, and R. R. Kerswell, Inertial enhancement of the polymer diffusive instability, *Journal of Fluid Mechanics* **981**, A2 (2024).
- [24] A. Morozov, Coherent structures in plane channel flow of dilute polymer solutions with vanishing inertia, *Phys. Rev. Lett.* **129**, 017801 (2022).
- [25] G. Buza, M. Beneitez, J. Page, and R. R. Kerswell, Finite-amplitude elastic waves in viscoelastic channel flow from large to zero reynolds number, *J. Fluid Mech.* **951**, A3 (2022).
- [26] H. J. Wilson and J. M. Rallison, Instability of channel flow of a shear-thinning White–Metzner fluid, *Journal of Non-Newtonian Fluid Mechanics* **87**, 75 (1999).
- [27] H. J. Wilson and V. Loridan, Linear instability of a highly shear-thinning fluid in channel flow, *Journal of*

- Non-Newtonian Fluid Mechanics **223**, 200 (2015).
- [28] H. Barlow, E. Hemingway, A. Clarke, and S. Fielding, Linear instability of shear thinning pressure driven channel flow, *Journal of Non-Newtonian Fluid Mechanics* **270**, 66 (2019).
 - [29] A. M. Grillet, A. C. Bogaerds, G. W. Peters, and F. P. Baaijens, Stability analysis of constitutive equations for polymer melts in viscometric flows, *Journal of Non-Newtonian Fluid Mechanics* **103**, 221 (2002).
 - [30] L. Picaut, O. Ronsin, C. Caroli, and T. Baumberger, Experimental evidence of a helical, supercritical instability in pipe flow of shear thinning fluids, *Physical Review Fluids* **2**, 083303 (2017).
 - [31] H. Bodiguel, J. Beaumont, A. Machado, L. Martinie, H. Kellay, and A. Colin, Flow enhancement due to elastic turbulence in channel flows of shear thinning fluids, *Physical Review Letters* **114**, 028302 (2015).
 - [32] R. Poole, Elastic instabilities in parallel shear flows of a viscoelastic shear-thinning liquid, *Physical Review Fluids* **1**, 041301 (2016).
 - [33] J. Cao and A. E. Likhtman, Shear banding in molecular dynamics of polymer melts, *Physical review letters* **108**, 028302 (2012).
 - [34] M. Mohagheghi and B. Khomami, Molecular processes leading to shear banding in well entangled polymeric melts, *ACS Macro Letters* **4**, 684 (2015).
 - [35] N. Spenley, M. Cates, and T. McLeish, Nonlinear rheology of wormlike micelles, *Physical review letters* **71**, 939 (1993).
 - [36] J. Yerushalmi, S. Katz, and R. Shinnar, The stability of steady shear flows of some viscoelastic fluids, *Chemical Engineering Science* **25**, 1891 (1970).
 - [37] M. A. Fardin, D. Lopez, J. Croso, G. Grégoire, O. Cardoso, G. H. McKinley, and S. Lerouge, Elastic turbulence in shear banding wormlike micelles, *Phys. Rev. Lett.* **104**, 178303 (2010).
 - [38] M. A. Fardin, T. J. Ober, V. Grenard, T. Divoux, S. Manneville, G. H. McKinley, and S. Lerouge, Interplay between elastic instabilities and shear-banding: three categories of Taylor–Couette flows and beyond, *Soft Matter* **8**, 10072 (2012).
 - [39] M. A. Fardin, T. Divoux, M. A. Guedeau-Boudeville, I. Buchet-Maulien, J. Browaeys, G. H. McKinley, S. Manneville, and S. Lerouge, Shear-banding in surfactant wormlike micelles: elastic instabilities and wall slip, *Soft Matter* **8**, 2535 (2012).
 - [40] J. F. Berret, G. Porte, and J. P. Decruppe, Inhomogeneous shear flows of wormlike micelles: a master dynamic phase diagram, *Phys. Rev. E* **55**, 1668 (1997).
 - [41] S. Lerouge, J. P. Decruppe, and J. F. Berret, Correlations between rheological and optical properties of a micellar solution under shear banding flow, *Langmuir* **16**, 6464 (2000).
 - [42] L. Bécu, D. Anache, S. Manneville, and A. Colin, Evidence for three-dimensional unstable flows in shear-banding wormlike micelles, *Phys. Rev. E* **76**, 011503 (2007).
 - [43] E. Cappelaere, J. F. Berret, J. P. Decruppe, R. Cressely, and P. Lindner, Rheology, birefringence, and small-angle neutron scattering in a charged micellar system: evidence of a shear-induced phase transition, *Phys. Rev. E* **56**, 1869 (1997).
 - [44] S. Lerouge, J. P. Decruppe, and C. Humbert, Shear banding in a micellar solution under transient flow, *Phys. Rev. Lett.* **81**, 5457 (1998).
 - [45] P. Rassolov, A. Scigliani, and H. Mohammadigoushki, Kinetics of shear banding flow formation in linear and branched wormlike micelles, *Soft Matter* **18**, 6079 (2022).
 - [46] R. Bandyopadhyay, G. Basappa, and A. K. Sood, Observation of chaotic dynamics in dilute sheared aqueous solutions of ctat, *Phys. Rev. Lett.* **84**, 2022 (2000).
 - [47] R. Ganapathy and A. K. Sood, Intermittency Route to Rheochaos in Wormlike Micelles with Flow-Concentration Coupling, *Phys. Rev. Lett.* **96**, 108301 (2006).
 - [48] M. E. Cates and S. M. Fielding, Rheology of giant micelles, *Adv. Physics* **55**, 799 (2006).
 - [49] P. D. Olmsted, Perspectives on shear banding in complex fluids, *Rheo. Acta* **47**, 283 (2008).
 - [50] P. D. Olmsted, O. Radulescu, and C.-Y. D. Lu, Johnson–Segalman model with a diffusion term in cylindrical Couette flow, *Journal of Rheology* **44**, 257 (2000).
 - [51] S. M. Fielding and P. D. Olmsted, Spatiotemporal oscillations and rheochaos in a simple model of shear banding, *Phys. Rev. Lett.* **92**, 084502 (2004).
 - [52] S. M. Fielding and P. D. Olmsted, Early stage kinetics in a unified model of shear-induced demixing and mechanical shear banding instabilities, *Phys. Rev. Lett.* **90**, 224501 (2003).
 - [53] S. M. Fielding, Linear instability of planar shear banded flow, *Phys. Rev. Lett.* **95**, 134501 (2005).
 - [54] S. M. Fielding and H. J. Wilson, Shear banding and interfacial instability in planar Poiseuille flow, *Journal of Non-Newtonian Fluid Mechanics* **165**, 196 (2010).
 - [55] H. J. Wilson and S. M. Fielding, Linear instability of planar shear banded flow of both diffusive and non-diffusive Johnson–Segalman fluids, *Journal of Non-Newtonian Fluid Mechanics* **138**, 181 (2006).
 - [56] M. Johnson and D. Segalman, A model for viscoelastic fluid behavior which allows non-affine deformation, *Journal of Non-Newtonian Fluid Mechanics* **2**, 255 (1977).
 - [57] A. E. Likhtman and R. S. Graham, Simple constitutive equation for linear polymer melts derived from molecular theory: Rolie–Poly equation, *Journal of Non-Newtonian Fluid Mechanics* **114**, 1 (2003).
 - [58] R. J. Gordon and W. R. Schowalter, Anisotropic fluid theory: a different approach to the dumbbell theory of dilute polymer solutions, *Trans. Soc. Rheol.* **16**, 79 (1972).
 - [59] R. Sureshkumar and A. N. Beris, Effect of artificial stress diffusivity on the stability of numerical calculations and the flow dynamics of time-dependent viscoelastic flows, *Journal of Non-Newtonian Fluid Mechanics* **60**, 53 (1995).
 - [60] J. M. Adams, S. M. Fielding, and P. D. Olmsted, Transient shear banding in entangled polymers: A study using the Rolie–Poly model, *Journal of Rheology* **55**, 1007 (2011).
 - [61] K. J. Burns, G. M. Vasil, J. S. Oishi, D. Lecoanet, and B. P. Brown, Dedalus: A flexible framework for numerical simulations with spectral methods, *Phys. Rev. Res.* **2**, 023068 (2020).
 - [62] C. Grand, J. Arrault, and M. Cates, Slow transients and metastability in wormlike micelle rheology, *Journal de Physique II* **7**, 1071 (1997).
 - [63] S. M. Fielding and P. D. Olmsted, Nonlinear dynamics of an interface between shear bands, *Phys. Rev. Lett.* **96**, 104502 (2006).

- [64] R. G. Larson, E. S. G. Shaqfeh, and S. J. Muller, A purely elastic instability in Taylor–Couette flow, *Journal of Fluid Mechanics* **218**, 573–600 (1990).

END MATTER

Appendix A: Identifying the instabilities as constitutive or PDI We now explain how we classify the linear instabilities of the main text as either constitutive or PDI. To identify a mode as constitutive, we show that its eigenmode can be continuously evolved into the 1D constitutive instability by changing the wavenumber k or the Weissenberg number W . It is useful to consider the most unstable wavenumber k^* , phase speed c_r^* and growth rate $\omega^* = k^* c_i^*$ as W varies in the JS and RP models in figures Figs. 4a,d at fixed $a = 0.5$ and $Z = 1000$ respectively. Both models show piecewise continuous k^* and c_r^* , with the discontinuities demonstrating a change in most unstable mode. All eigenmodes were found using a resolution of $N_y = 256$ Chebyshev polynomials, and we verified that a resolution of $N_y = 384$ produced the same results.

The JS model has only 1 change in mode, at $W = 45$, as seen in Fig. 4a. We now identify the mode at $W < 45$ as constitutive. When $W < 2.8$, the most unstable mode is 1D as it has $k^* = 0$, and hence it is the 1D constitutive instability associated with non-monotonicity. As W increases into $2.8 < W < 45$, k^* increases, meaning the instability becomes 2D, but the continuity of k^* and c_r^* demonstrates that this instability is the same mode as the 1D constitutive instability. Hence, this is still constitutive in nature. This mode strongly resembles the shear thinning linear instability of Grillet *et al.* [29] (compare the eigenmodes in Fig. 4c at $W = 6, 15, 30$ with Fig. 15 of Ref. [29]), where the polymer stress and streamfunction were tilted in the fluid bulk. It has $c_r^* = 0$, meaning the most unstable mode is stationary. We now consider the most unstable mode for $W > 45$, and see that it exists at larger k^* and has a phase speed of the same order of magnitude as the boundary speed $c_r^* \sim W$ (see Fig. 4a). We identify this mode as PDI, as it is a boundary mode resembling PDI (compare the eigenmode at $W = 100$ in Fig. 4c to Fig. 3a in Ref. [16]) and it scales like $k^* \sim \varepsilon^{-1/2}$ and $\sigma^* \sim \varepsilon^0$ as $\varepsilon \rightarrow 0$ (unshown). We plot dispersion relations at various W in Fig. 4b, and the eigenfunctions of the most unstable modes in Fig. 4c.

The RP model has 2 changes in mode, as can be seen by the discontinuities in k^* in Fig. 4d; however, the modes at the lowest and highest W are the same. We demonstrate that the most unstable mode for both $W < 5.8$ and $W > 6.9$ is constitutive by considering the dispersion relation at various W (see Fig. 4e). At $W = 20$, the mode that is most unstable at $k = k^*$ originates from the 1D constitutive instability at $k = 0$, as kc_i and c_r are continuous as k varies in the interval $(0, k^*]$ (see

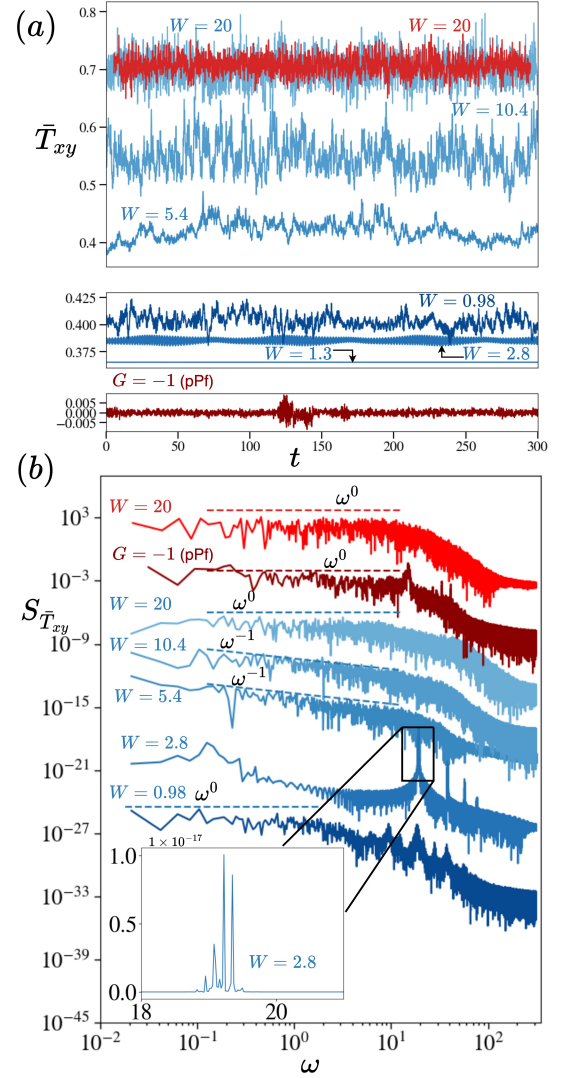


FIG. 3. (a) Timeseries of the spatially-averaged shear stress \bar{T}_{xy} for all states plotted in Fig. 2. (b) The frequency spectra $S_{\bar{T}_{xy}}$ of the time-dependent timeseries over $T = 300$. For clarity, the spectra are rescaled by constants to prevent overlapping in the figure. The JS model is shown in blue while the RP model is shown in red. The JS model suggests temporal chaos with $S_{\bar{T}_{xy}} \sim \omega^{-1}$ or, $S_{\bar{T}_{xy}} \sim \omega^0$ depending on W , and it shows a quasi-periodic state at $W = 2.8$, while the RP model shows temporal chaos with $S_{\bar{T}_{xy}} \sim \omega^0$ in both pCf and pPf.

Fig. 4e, $W = 20$). The most unstable mode in Fig. 4d for $W > 6.9$ is therefore constitutive. In the narrow interval of $5.8 < W < 6.9$, an additional ‘mode A’ becomes most unstable. As it is only most unstable in such a small region here, we do not investigate it further. For $W < 5.8$, mode A is suppressed, leaving the constitutive mode as the only instability at this W in the dispersion relation at $W = 4$ (see Fig. 4e). Hence, the most unstable mode shown in Fig. 4d for $W < 5.8$ is also constitutive. We plot the most unstable eigenmodes at various W in Fig. 4f, and again see that the constitutive instability re-

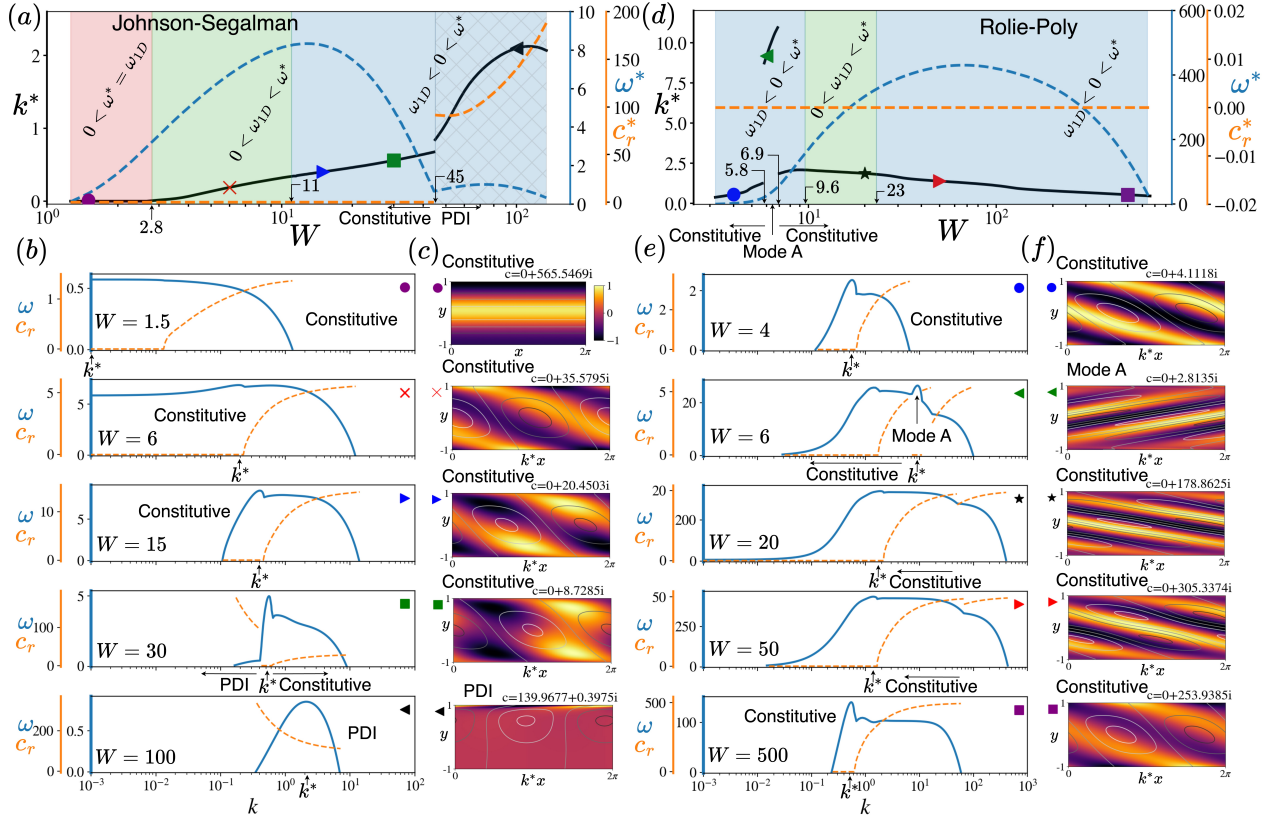


FIG. 4. (a-c) Identifying most unstable modes in the JS model with $\delta = 10^{-2}$, $\varepsilon = 10^{-3}$ and $a = 0.5$. (a) shows the most unstable wavenumber k^* (solid black), the growth rate ω^* (dashed blue) and the phase speed c_r^* (dashed orange) along the dashed vertical line of Fig. 1c, with background colours as in Fig. 1c. (b) Dispersion relations showing the growth rate ω (solid blue) and phase speed c_r (dashed orange) against wavenumber k at the various W marked by symbols in (a). (c) The most unstable eigenmode at each W with colour denoting the trace $\Sigma_{xx} + \Sigma_{yy} + \Sigma_{zz}$ and contours showing the streamfunction. Colour scales for all eigenmodes are as in the top eigenmode of (c), with mode amplitude arbitrary. Constitutive instabilities resemble the shear thinning instability of Ref. [29]. (d-f) show the same in the RP model when $\delta = 10^{-4}$, $\varepsilon = 10^{-3}$ and $Z = 1000$.

sembles the shear thinning instability [29]. All of these are stationary modes with $c_r^* = 0$.

We have demonstrated that the most unstable 2D linear instability present in the JS fluid transitions from constitutive to PDI as W increases for Neumann stress boundary conditions, while in the RP fluid the only identified instability that exists over a wide range of W is constitutive. In both models the 2D constitutive mode strongly resembles the shear thinning instabilities of [29]. We verified robustness by checking these results in both models with stress diffusion-free boundary conditions (unshown). In addition, we checked that changing δ in the JS model to $\delta = 3 \times 10^{-3}$, and in the RP model to $\delta = 10^{-3}$ did not change the most unstable modes substantially (unshown). At this δ in the RP model, mode A is no longer most unstable at $W \sim 6$, but a different mode is most unstable at $80 < W < 120$. As this is not robust to δ , we do not analyse it further.

Appendix B: Demonstrating Simulations are Chaotic

The chaotic properties of the ultimate states plotted in Fig. 2 are verified in Fig. 3. We show the timeseries of

the spatially-averaged shear stress \bar{T}_{xy} in Fig. 3a, while its temporal power spectra is shown in Fig. 3b. The broadband power spectra are consistent with temporal chaos in pCf for $W = 20.0, 10.4, 5.4$ and 0.98 in the JS model and at $W = 20.0$ in the RP model. The JS model at $W = 2.8$ is quasi-periodic however, as it has distinct peaks in its spectra at incommensurate frequencies (see the inset of Fig. 3b). In addition, these suggest temporal chaos in pPf in the RP model with imposed pressure gradient $G = -1$ and entanglement number $Z = 50$. This pPf turbulence has lower energy than in the pCf case, with the \bar{T}_{xy} timeseries shown in Fig. 3a for pPf having a standard deviation of 0.0013. Upon increasing the entanglement number to $Z = 100$ and $Z = 500$ this standard deviation increases to 0.0035 and 0.0036 respectively (unshown). For comparison, the standard deviation in the pCf case at $W = 5.4$ was 0.0165. The difference in magnitude of the fluctuations between the pCf and pPf case is perhaps due to the fact that in pCf entire shear bands drift in the wall-normal direction, unlike in the pPf case where bands are localised close to the boundary.